meson at about 575 MeV/c^2. About 520 weighted events above background are thus expected; the data show only about 40 net weighted events above the Olsson-Yodh curve within the mass region 540–610 MeV/c^2. If the theoretical curve were an exact representation of the background, this observed excess would amount to about 1 standard deviation and would correspond to a cross section of 0.06 mb.

No bumps of the size and location reported by others[5] in this region are observed in these data. For a peak narrower than our experimental resolution, our upper limit (99% confidence level) on cross section is about 0.1 mb.

We conclude that there is no evidence for a meson created in π^+p at 968 MeV/c and decaying into $\pi^+\pi^0$.

ACKNOWLEDGMENTS

We wish to thank Miss Eva Bonis and members of the scanning group for their diligent work in scanning and measuring these events and also Miss Dina Dubin for her expert work on the reconstruction and calibration programs. We thank Lyman Stinson for his excellent technical work and also the members of the BNL-AGS staff (especially Dr. Hildred Blewett) and crew for their expert support during the experimental run.

PHYSICAL REVIEW VOLUME 164, NUMBER 5 25 DECEMBER 1967

Backward Photoproduction of π^0 in the Region of the P_{33} Pion-Nucleon Resonance

M. CROISSIAUX, E. B. DALLY,* R. MORAND, AND J. P. PAHIN
Laboratoire de l'Accélérateur Linéaire, Orsay, France and Institut de Recherches Nucléaires, Strasbourg, France

AND

W. SCHMIDT
Institut für Experimentelle Kernphysik, Kernforschungzentrum, Karlsruhe, Germany

(Received 1 June 1967)

The π^0 photoproduction cross section has been measured at 180° for photon energies from 220 to 380 MeV, in steps of 20 MeV, by detecting the recoil proton at 0°. The statistical accuracy of the measurements varies between 3 and 7%, depending on the energy. Absolute cross sections have been deduced from a comparison of the measurements with electron-proton scattering. The experimental data are compared with theoretical results calculated from fixed-momentum-transfer dispersion relations. Special attention is paid to the prediction of the multipoles at the first resonance, namely, $E_{1+}^{3/2}$, $M_{1+}^{3/2}$, and $E_{0+}^{\pi^0}$ to obtain agreement with experiment.

I. INTRODUCTION

UNTIL recently the experimental information about π^0 photoproduction from the proton in the region of the first pion-nucleon resonance $\Delta(1236)$ has been very limited. The functional dependence on the photon energy E or the production angle θ (in the c.m. system) has been established in the threshold region and only in a few other cases. There are recent and old data available from the counter experiments done at Moscow,[1] Glasgow,[2] and from the work with emulsion plates at Munich,[3] which give the first three coefficients A, B, and C of the expansion of the differential cross section (in the c.m. system)

$$d\sigma(E,\theta)/d\Omega = A + B\cos\theta + C\cos^2\theta + D\cos^3\theta + \cdots \quad (1)$$

up to $E=240$ MeV. At higher energies, measurements[2–4] at $\theta=90°$ yielded the energy dependence of A in the region of the first pion-nucleon resonance. But all other data do not give sufficient information for the asymmetry coefficients B and D. The present measurements yield data in a kinematical region especially suited for a further check of the existing theories. Furthermore,

* Present address: W. W. Hansen Laboratories, Stanford University, Stanford, California.

[1] V. I. Goldansky, B. B. Govorkov, and R. G. Vasilkov, Nucl. Phys. **12**, 327 (1959); R. G. Vasilkov, B. B. Govorkov, and V. I. Goldansky, Zh. Eksperim. i Teor. Fiz. **37**, 11 (1959) [English transl.: Soviet Phys.—JETP **10**, 7 (1960)]; B. B. Govorkov, S. P. Denisov, A. I. Lebedev, and E. V. Minarik, Zh. Eksperim. i Teor. Fiz. **44**, 1463 (1963) [English transl: Soviet Phys.—JETP **17**, 983 (1963)]; B. B. Govorkov, S. P. Denisov, A. I. Lebedev, E. V. Minarik, and S. P. Kharlamov, Zh. Eksperim. i Teor. Fiz. **47**, 1199 (1964) [English transl: Soviet Phys.—JETP **20**, 809 (1965)].

[2] D. B. Miller and E. H. Bellamy, Proc. Phys. Soc. (London) **81**, 343 (1963).

[3] W. Hitzeroth, in *Proceedings of the International Symposium on Electron and Photon Interactions at High Energies*, edited by G. Höhler *et al.* (Deutsche Physikalische Gesellschaft, Hamburg, 1965), Vol. II, 209.

[4] R. L. Walker, D. C. Oakley, and A. V. Tollestrup, Phys. Rev. **97**, 1279 (1955); D. C. Oakley and R. L. Walker, Phys. Rev. **97**, 1283 (1955); W. John and G. Stoppini, Nuovo Cimento **6**, 1206 (1957); W. S. McDonald, V. Z. Peterson, and D. R. Corson Phys. Rev. **107**, 577 (1957); R. Smythe, B. M. Worlock, and A. V. Tollestrup, Phys. Rev. **109**, 518 (1958); C. Bacci, C. Mencuccini, G. Penso, A. Reale, G. Salvini, V. Silvestrini, M. Spinetti, and B. Stella, Frescati Report No. INF-66165, 1966 (unpublished).

they will supplement in the backward direction the recent measurements at other angles done at Bonn, the first results of which have been already reported.[5]

On the other hand, the theoretical interpretation of π^0 photoproduction from the proton is considerably more difficult than for π^+ production. In π^0 production there is one large contribution to the total amplitude coming from the first resonance, the resonant magnetic dipole amplitude $M_{1+}^{3/2}$, which at the present stage of the theory can be calculated within 10% around the resonance. But the background amplitudes, which are important at threshold and at higher energies because of their interference with the large multipole $M_{1+}^{3/2}$, consist of several small contributions. Their calculation turns out to be more uncertain in the framework of the present theoretical approach, which is based mainly on fixed-t dispersion relations, than in π^+ production, where the one large s-wave contribution dominates the background. Therefore, the interpretation of measurements made in the backward (or forward) direction, which are sensitive to the s-p interference terms, depends strongly on the approximations in the dispersion relations. For example, in these terms the electric quadrupole excitation $E_{1+}^{3/2}$ of the first resonance is important and is presently attracting theoretical interest.

The measurement of the cross sections of the reaction

$$\gamma+p\rightarrow\pi^0+p$$

at $\theta=180°$ is experimentally difficult for the energy region around the first pion-nucleon resonance. We have chosen to detect the recoiling protons. Because of the two-body nature of the kinematics, the detection system must be in the direction of the photon beam, and hence, of the electron beam which produces it.

In Sec. II, the experimental method is outlined. Section III explains the details of the apparatus. In Sec. IV, the data-accumulation procedures are described. The corrections made to the data are indicated in Sec. V. Section VI gives the experimental results and the errors on the cross sections. In Sec. VII, the theory of the π^0 photoproduction is developed. The experimental results are used to check a new evaluation of the partial-wave dispersion relations for the first pion-nucleon resonance.

II. EXPERIMENTAL METHOD

The measurements of the π^0 photoproduction cross section on hydrogen at 180° were performed[6] by measuring the momentum of the recoil proton from the process at zero degrees, and then detecting it. The technique which was applied was the same as that used for the measurements of electron-proton scattering at 180°,[7] and then applied to several other experiments.[8–10] A spectrometer is placed at zero degrees, and the electron beam from the accelerator, after passing through the target, enters directly into the vacuum chamber of the spectrometer along with the particles produced by the reaction in the target. Reactions which produce particles of the opposite charge from the beam, thus enabling a magnetic field to bend beam and reaction particles in opposite directions, are necessary in order to prevent overwhelming quantities of beam particles from reaching the detectors.

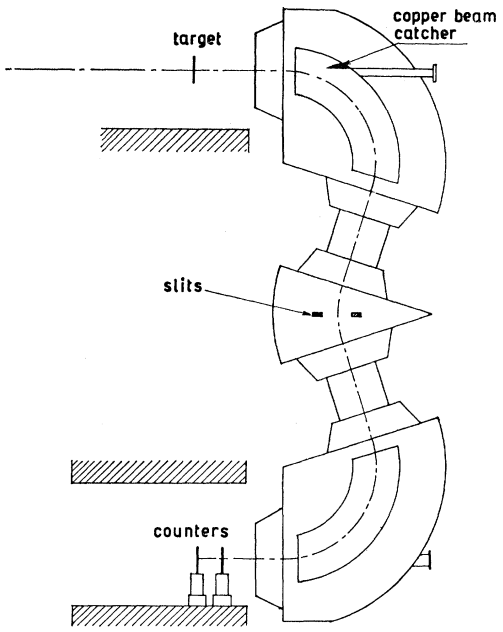

FIG. 1. Triple focusing spectrometer, showing the location of the beam catcher and transverse and radial slits.

As an aid to reducing background particles arising from the stopped beam, a slug of copper 3 cm thick was placed in the spectrometer vacuum chamber (Fig. 1) in such a way as to stop particles backscattered from the point of impact of the electron beam. Its position was such that it was not struck by the upward curving electron beam, and did not interfere with particles in orbits that led to the detectors.

For the present experiment, the momentum of the protons was so large that the maximum energy of the positrons produced by the beam lacked the momentum necessary to be transmitted by the spectrometer. The

[5] G. Fischer, H. Fischer, H. J. Kämpgen, G. Knop, P. Schulz, and H. Wessels, in *Proceedings of the Thirteenth Annual International Conference on High-Energy Physics, Berkeley, California, 1966* (University of California Press, Berkeley, 1967); and (private communication).

[6] M. Croissiaux, E. B. Dally, R. Morand, J. P. Pahin, and W. Schmidt, Bull. Am. Phys. Soc. **12**, 9 (1967).

[7] P. A. M. Gram and E. B. Dally, Bull. Am. Phys. Soc. **7**, 489 (1962); P. A. M. Gram, thesis, Stanford University, 1965 (unpublished).

[8] D. Frerejacques, D. Benaksas, and D. Drickey, Phys. Rev. Letters **12**, 1 (1964).

[9] J. C. Bizot, J. Perez y Jorba, and D. Treille, in Ref. 3, p. 227.

[10] A. Browman, B. Grossetete, and D. Yount, Phys. Rev. **143**, 899 (1965).

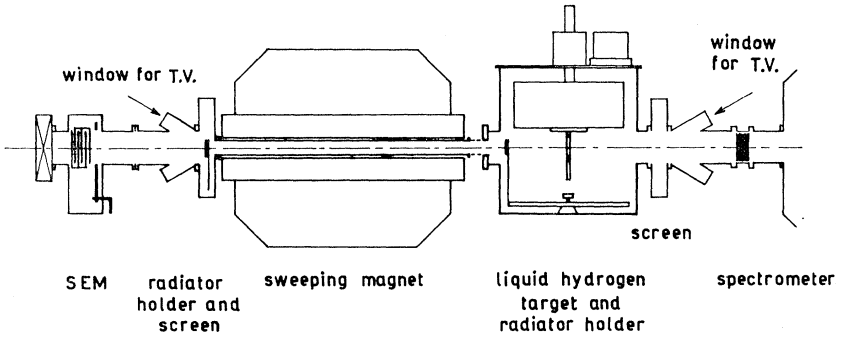

FIG. 2. Experimental setup. Electron beam is coming from the left. Photon beam produced by one of the radiators strikes the hydrogen target. Protons emitted then enter directly into the spectrometer for detection. Beam monitor, electron sweeping magnet, and apparatus for controlling the beam centering are also indicated.

absolute values of the photoproduction cross sections were determined by measuring the well-known elastic electron-proton scattering cross sections for each point. The incident electron energy was adjusted to produce the elastic peak of the recoil proton at exactly the same momentum as for the protons arising from a particular photoproduction point. In this way, uncertain factors such as spectrometer solid angle and detector efficiency cancelled in the ratio. Figures 1 and 2 show the experimental setup, the details of which will be described in the following section.

III. EXPERIMENTAL DETAILS

A. Accelerator

The electron beam for this experiment was produced by the linear electron accelerator facility at the Faculté des Sciences, Orsay. After acceleration the electrons entered a three-magnet (isochronic) deviation system where the energy spread of the beam was defined by slits. This system presented a focused beam at the target. Auxiliary beam-steering and focusing coils were also used for fine beam adjustments. The energy calibration for the incident beam was made using a floating-wire method, and had an estimated error of 0.5%. A proton resonance probe which was calibrated by comparison to the floating-wire measurement, was used to monitor the field setting of the deviation system, and permitted the accurate resetting of the field for repeated measurements.

B. Photon Beam

The photon beam was produced from the bremsstrahlung process by passing electrons through a thin target (radiator). The photon spectrum which is produced has been calculated using the Bethe-Heitler treatment. In the present experiment, the spectrum was calculated using the bremsstrahlung program of Alvarez[11] as modified by Allton,[11] which treats the case of a thick radiator. This calculation includes corrections for the straggling of the electrons within the radiator and for reabsorption of the photons through pair production. Corrections for screening and Coulomb effects are included. The estimated accuracy of these calculations is $\pm 1\%$.

Two different experimental techniques were used (see Fig. 2). The first utilized a pure photon beam to produce the π^0, while in the second both the electron and photon beams passed through the target. The reasons for using the two methods were practical ones. Making measurements with the pure photon beam is more desirable. There are no large subtractions and corrections to be made for the electroproduction process and the background is less because the electron beam does not produce large quantities of neutrons in the vacuum chamber of the spectrometer, close to the detectors. However, to have the pure photon beam, the electron beam must be swept away ahead of the target by a sweeping magnet. This necessitates placing the radiator quite far from the target. The multiple scattering of the electron beam in the radiator produces a diverging photon beam which can become large in diameter at the target and in the spectrometer, for reasonable radiator thicknesses, especially at lower beam energies. This in turn causes a difference in the collection efficiency of the recoil photoproduction protons in the normalization measurements. Hence, for this experiment, both methods were used.

At the lower energies (220–300 MeV) the electron beam was passed through the target. In this region the photoproduction cross section is small and thus a thicker radiator is desirable to obtain reasonable counting rates. In addition, it was found that the electroproduction cross section is relatively smaller in this region than at higher energies so that electroproduction measurements needed for background subtraction required less time than they would have at the higher energies (300–380 MeV).

To produce the photon beam, thin Cu or Al radiators were mounted ahead of the target. The surface density of these radiators was determined by measuring the area and weighing them. The estimated error of the surface density is 0.8%. Aluminum radiators of thickness approximately 0.3 and 0.6% radiation lengths were used for the ditched-beam experiments and were mounted before the sweeping magnet. Copper radiators of 3 and 6% radiation lengths for the unditched-beam experi-

[11] R. Alvarez, Stanford University Internal Report No. HEPL-228, 1961 (unpublished); Alvarez's program was modified and rewritten for IBM 7090 computer by E. Allton (private communication).

ments were mounted in the scattering chamber just ahead of the target. The distances of the radiators from the target was approximately 1.80 and 0.20 m for the Al and Cu radiators, respectively.

All measurements were made with a constant k/E_0, where k is the photon energy in the laboratory system, and E_0 the incident electron energy. A rather large k/E_0 of 0.85 was used in order to keep the total number of photons with energy greater than k as small as was reasonable, because all such photons can contribute additional background protons.

C. Beam Monitoring

The electron beam monitoring was done with a secondary-emission monitor (SEM), which was calibrated using a Faraday cup. The efficiency of the cup was $99.8\%\pm0.2\%$.[12] This SEM, which was mounted in the beam pipe upstream from the experiment (see Fig. 1), had seven emitting and six collecting foils which yielded an efficiency of approximately 22%. Each foil was 1.5 μ thick. The foils contributed a negligible amount of multiple beam scattering and photon production.

A second SEM was mounted in such a way as to intercept the electron beam for the experiments in which the beam was ditched. This second SEM, with an efficiency of approximately 30%, was pumped continuously to a very high vacuum with a vacion pump, which allowed very good long-term stability. The second SEM was used to check continuously the response of the integrated charge of the first SEM. Its efficiency fluctuated less than 1% during several hours. As a result of these observations, the efficiency of the beam-pipe SEM was assumed to have varied less than 1% during the runs in which the electron beam was not swept, but passed directly into the spectrometer vacuum chamber.

Efficiency measurements of the SEM were made routinely at the beginning and at the end of the data runs of each proton elastic peak and photoproduction point. Although the absolute value of the efficiency was not needed because the photoproduction cross sections were measured relatively to the elastic electron-proton scattering, such measurements were necessary because of the slight energy variation of the efficiency[13] of the SEM's. (A lower incident energy was required for the elastic electron-proton scattering peak corresponding to protons of the same momentum as those from photoproduction.) In addition, they served as a control of the stability of the entire beam-monitoring system. For each efficiency measurement it was necessary to turn off the spectrometer magnetic field (and ditching magnetic field, if used) in order for the electron beam to reach the Faraday cup.

[12] D. Isabelle, Onde Electrique **421**, 354 (1962).

[13] F. Bumiller and E. B. Dally, in *Proceedings of an International Conference on Instrumentation in High-Energy Physics* (Interscience Publishers, New York, 1961), p. 304.

The collected charge was measured using electronic integrators.[14] They have been checked using a precision current source and the variation of their response was of the order of $\pm0.5\%$.

D. Target

All measurements were performed with a liquid hydrogen target. The target was approximately 2 cm thick and presented a surface with dimensions 8×5 cm to the photon beam. 12-μ-thick stainless-steel foils were used as target walls. Originally constructed as a condensing type target,[15] it was modified by connecting the liquid hydrogen reservoir directly to the target chamber. Two positions were possible; namely "target full" and "target empty" with two 12-μ stainless-steel foils simulating the full-target walls.

E. Spectrometer

The spectrometer used for this experiment was a triple-focusing type with three magnets (see Fig. 1).[16] Because of its configuration, its properties as a "filter" for background particles scattering several times from the vacuum chamber walls were ideal. In addition, the detectors were well shielded by 4.10 m of iron, and the separation of the detectors from the point of impact of the beam inside the vacuum chamber was quite long. This reduces neutron background in the detectors. A calibration curve for the spectrometer has been made using the floating-wire method.[16] The estimated error of this calibration is $\pm0.2\%$. The stability of a field setting was checked using Hall probes, and field drifts were observed to be negligible.

The entire system, consisting of radiators, deflecting magnet, target, and spectrometer, was aligned with a transit by sighting through the exit port of the vacuum chamber.

The solid angle was defined in the following way: To be sure that external entrance slits really defined the solid angle at the higher momentum settings where the iron is saturating, their openings should be very small. However, with such openings, an excessive background would result because the fringes of the photon beam could strike the slits. For that reason, a tungsten slit of 6 cm opening was put in the horizontal symmetry plane of the spectrometer (Fig. 1) to define a horizontal slit opening. In the vertical direction, a lead baffle 10 cm high was placed at the entrance of the magnet, and it did not cause any background from the photon beam.

Before taking a measurement, a check was made to test the positions of these diaphragms. Counting rates were registered for the electron and photon beam centered on the target and then by moving them around

[14] Orsay Internal Report No. Service Electronique 6-65, 1965 (unpublished).

[15] V. Round, D. Benaksas, and P. Bounin, Nucl. Instr. Methods **26**, 348 (1964).

[16] J. Dupin, thesis, Orsay, 1966 (unpublished).

the center of target in the vertical and horizontal plane. The counting rate was constant within 4% in a square region 2 cm on a side centered about the center of the target.

Because of this slit configuration, the solid angle was not known just from geometry. It is for this reason that the photoproduction cross section was determined by measurement relative to electron-proton scattering. The product of solid angle by detector efficiency calculated from elastic electron-proton peaks was constant as a function of momentum.

The optical properties of the spectrometer were also determined by the floating-wire measurements.[16] In particular, the focal point was located. For this spectrometer, its position varied as a function of the momentum setting, as well as of the momentum resolution as determined by a radial slit placed in the horizontal symmetry plane of the system (see Fig. 1). Therefore, the detectors were placed in a position appropriate for the photoproduction point being measured. Finally, the entire system of beam pipe, ditching magnet, target, and spectrometer constituted a continuous vacuum system at a pressure less than 1×10^{-5} mm Hg.

F. Detectors

The detector system was composed of two thin plastic scintillators (4 and 6 mm thick) arranged to form a telescope. The scintillators (160×100×4 mm for the front, 160×100×6 mm for the back) were connected optically by light guides to two 56 AVP photomultipliers. The light guides were designed according to the principles outlined in Ref. 17, which says that the optimum light guide must be tapered in such a way that the cross-sectional area is constant. The detected proton energies varied from 55 to 155 MeV and the energy losses varied, respectively, from 4.5 to 2 MeV in the first counter and from 8 to 3.5 MeV in the second counter.

Tests made with the use of an α-particle source showed that the output pulse of the photomultipliers varied little with the position of the source. The proton pulse-height spectra were well-defined and narrow (see Fig. 3), and assured an efficient detection of the protons. Because the detectors were thin and placed close together, there were no scattering losses of protons. To be recorded, a particle had to pass through both of them, and the photomultiplier pulses had to be in time coincidence. In addition solid-state light pulsers were mounted on the photomultipliers and were used to check their performance as well as to make the time alignment of the pulses.

G. Electronics

An anode and a dynode pulse from each photomultiplier were sent through fast coaxial cables to the counting room. The dynode pulses were stretched and used to observe the pulse-height spectra in a multichannel analyzer. The anode pulses were used for the coincidence and counting logic. Fast electronic circuits, manufactured by Chronetics, Inc., were used to discriminate and shape the pulses, which were then injected into a fast-coincidence module. The entire set of modules was gated by a synchronization pulse from the accelerator. 100-mc scalers were used to count the individual and coincidence pulses. An output from the discriminator unit was stretched and shaped, and used as a gated input to the multichannel analyzer to indicate the place where the proton pulse-height spectra were cut by the discriminator settings. These are shown in Fig. 3.

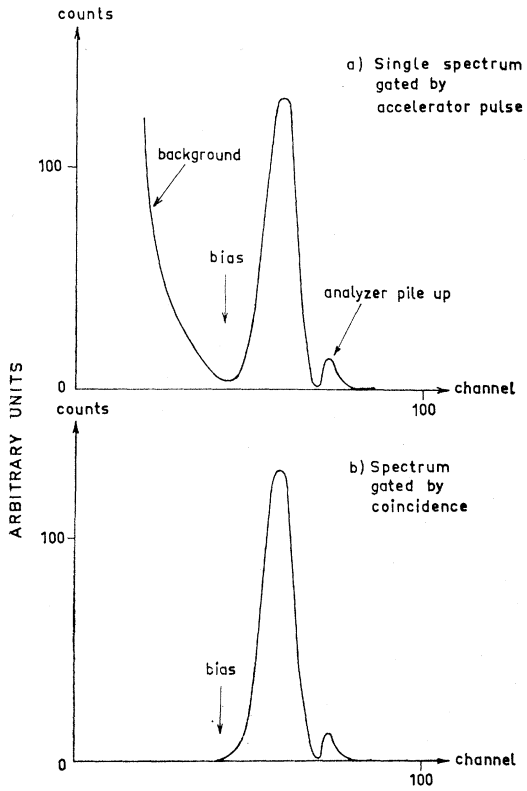

FIG. 3. Proton pulse-height spectra, showing discriminator setting.

Detection and scaling efficiency were assumed to be 100% for all measurements. The upper limit of the counting rate that was allowed was 15 per sec and was often less. This rate was low enough to give a negligible counting-rate correction. Such a conservative rate was used because of the large variations of shape, structure, and length of the beam pulses from the machine during a run. To count at a very high rate and to apply the normal counting loss corrections under such circumstances would have been meaningless. The accidental coincidence rate, calculated from singles counting rates, was negligible.

[17] M. A. Meyer and N. S. Wollmarans, Nucl. Instr. Methods, 25, 134 (1963).

IV. DATA

A. Procedure

At the beginning of each run, a cable delay curve was made to align the coincidence timing of the photomultipliers. The width of the delay curve was approximately 20 nsec.

Before each datum point was begun, pulse-height spectra were accumulated, and the discriminators adjusted to give a cutoff position low enough to avoid the loss of proton counts. Then, the fields of the spectrometer and sweeping magnet were reduced to zero and the SEM was calibrated by comparison with the Faraday cup.

For the measurement of the π^0 photoproduction, a series of four measurements was always made, in no particular sequence, for the runs with and without ditched electron beam. They were: target full, with and without radiator (N_1,N_3); target empty, with and without radiator (N_2,N_4).

With the electron beam passing through the target, the counting rates can be expressed in the following way:

$$\text{radiator:}\quad N_1=P_{\gamma+\gamma'}(H+W)+C_{\gamma+\gamma'}(H+W)+fE_e(H+W)+gR_e(H+W), \quad (2)$$

$$\text{radiator:}\quad N_2=P_{\gamma+(\gamma'-H/2)}(W)+C_{\gamma+(\gamma'-H/2)}(W)+fE_e(W)+gR_e(W), \quad (3)$$

$$\text{no radiator:}\quad N_3=P_{\gamma'}(H+W)+C_{\gamma'}(H+W)+E_e(H+W)+R_e(W), \quad (4)$$

$$\text{no radiator:}\quad N_4=P_{\gamma'-H/2}(W)+C_{\gamma'-H/2}(W)+E_e(W)+R_e(W), \quad (5)$$

where the following notations are used: P denotes the photoproduction contribution; C the Compton effect; E the electroproduction; R the contribution due to the radiative tail of the electron-proton scattering, H the hydrogen target; W the target walls; γ the photon beam due to the real radiator; and γ' the photon beam produced by the electron beam in the beam monitor, one target wall, and the radiator equivalent of the hydrogen target. From now on, these radiators will be called the "external" radiator. The letter e refers to electrons. The symbols f and g are coefficients which take into account the smearing of the spectrum of the electron beam at lower energies, which is caused by its passage through the radiator. They will be discussed subsequently. With the sweeping magnet, the E and R contributions are cancelled out and those from γ' are reduced by a large factor.

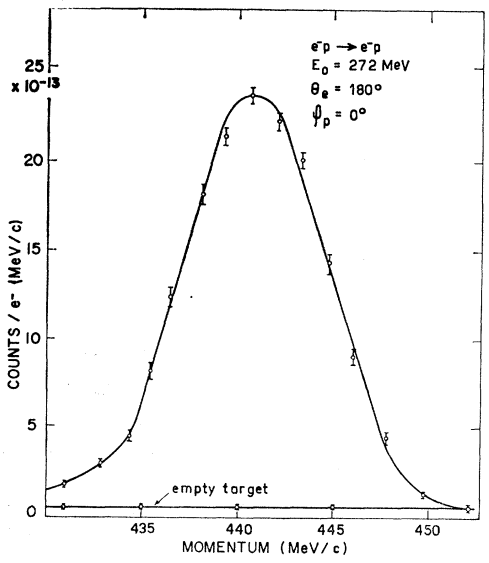

FIG. 4. Example of an e-p elastic-scattering peak for detection of protons at zero degrees.

The photoproduction counting rate is calculated from the quantities

$$N_{\text{in}}=N_1-N_2, \quad (6)$$

$$N_{\text{out}}=N_3-N_4, \quad (7)$$

and

$$P_\gamma(H)=N_{\text{in}}-N_{\text{out}}-(f-1)E_e(H)-(g-1)R_e(H)-C_\gamma(H). \quad (8)$$

With these measurements, the electroproduction contribution can also be determined:

$$E_e(H)=N_{\text{out}}-P_{\gamma'}(H)-C_{\gamma'}(H)-R_e(H)-P_{H/2}(W)-C_{H/2}(W). \quad (9)$$

After such a series of measurements, the magnetic fields were turned off and the SEM recalibrated. The electron energy was reduced to such a value as to give recoil protons from elastic electron-proton scattering which had the same momentum as the proton from photoproduction. The SEM was recalibrated and the elastic peak measured (Fig. 4). This was followed by another SEM calibration.

The statistical accuracy of the photoproduction data after the subtraction of the background and electroproduction contributions varied from 3 to 8% for the various points measured. Subtraction problems are explained in the next section.

B. Calculations

After subtraction of the background and electroproduction contributions, the number of proton counts coming from pion photoproduction is (dropping the integral and using finite quantities)

$$N_p=\frac{d\sigma^*(k,\theta)}{d\Omega^*}\frac{d\Omega^*}{d\Omega}\Delta\Omega n_v t N_i n_\tau \Phi(E_0,k)\Delta k. \quad (10)$$

Here, $d\sigma^*(k,\theta)/d\Omega^*$ is the cross section in the c.m. system for production of a π^0 at angle θ by a photon with laboratory energy k, $d\Omega^*/d\Omega$ is the solid-angle transformation from the c.m. to the laboratory system,

$\Delta\Omega$ is the solid angle accepted by the spectrometer, n_v is the number of protons/cm^3 in the target, t is the target thickness, N_i is the number of electrons, n_r is the number of atoms/cm^2 in the radiator, $\Phi(E_0,k)$ is the cross section for the production of a γ ray of energy k by an electron with incident energy E_0, and Δk is the effective slice of the bremsstrahlung spectrum giving rise to the photoproduced protons transmitted by the spectrometer. The product of the last four factors yields the number of photons of energy k in the interval Δk.

Now,

$$\Delta k=(\partial k/\partial p)\Delta p, \tag{11}$$

where $\partial k/\partial p$ is calculated from the kinematics, and Δp is the spread of proton momenta accepted by the spectrometer.

The total number of protons arising from the elastic scattering is given by integrating the peak, and including part of the radiative tail to a cutoff point of 3 or 4% below the peak center. The counts/e-(MeV/c) are related to the scattering cross section by

$$N_p=\int_{p_l}^{p_u}\frac{N(p)dp}{p(\Delta p/p)N_i}=\left(\frac{d\sigma}{d\Omega}\right)\Delta\Omega n_v t, \tag{12}$$

where p_l and p_u are, respectively, the lower and upper cutoffs of the proton spectrum. Here the quantities are the same as above except that the elastic-scattering cross section is given in the laboratory system and corrected for the radiative effects with the cutoff at p_l.

Values of the elastic proton scattering cross section were calculated using the Rosenbluth formula for the squares of the momentum transfer between 2.64 and 7.5 F^{-2}. The form factors for it were obtained using the best-fit parameters to a three-pole fit found from experiment by Janssens *et al.*[18]

V. CORRECTIONS TO THE DATA

The corrections to be included are of two kinds and come from normalization problems and from subtractions of other processes already mentioned. The elastic scattering was corrected for radiative effects using the calculation of Meister and Yennie.[19] This amounted from 9 to 11% for these data. An additional radiative correction of about 2%,[20] arising from the target acting as a radiator, was also applied. Corrections applied to the photoproduction data are as follows:

(a) The Compton effect on the proton has to be taken into account. Measured values of DeWire *et al.*[21] and calculations by Contogouris[22] have been used to estimate the correction. It varies from 1 to 3%. The corrections indicated up to now are the only ones necessary when the sweeping magnet is used. When the beam is not ditched, additional corrections must be made.

(b) There is a contribution from the electroproduction process. This reaction has been measured [Eq. (7)]. That contribution differs from the one measured in the (N_1-N_2) measurement [Eq. (6)] because of the presence of the radiator. When the radiator is present, the bremsstrahlung process causes a degradation of the spectrum of the electron beam. The beam spectrum is no longer approximately monoenergetic, but has a tail extending to lower energies. The factor f [Eq. (8)] takes this effect into account, where

$$f=\int_k^{E_0}W(E,E_0,t)M(E,p)dE\Big/M(E_0). \tag{13}$$

$W(E,E_0,t)dE$ is the probability for an electron with incident energy E_0 of having an energy E after passing through a radiator of thickness t (t in radiation lengths). This has been obtained from the Bethe-Heitler spectrum.[23] $M(E,p)$ is the electroproduction cross section for an electron of incident energy E with a fixed momentum p for the detected proton. This cross section is not known; therefore, it was measured as a function of E at fixed momentum and angle of the spectrometer, and normalized by the quantity $M(E_0)$, which is in fact $E_e(H)$ [Eq. (8)]. The quantity f was found to be about constant. The value varies from 0.89 to 0.92, depending on the point.

(c) The contribution of elastic and inelastic e-p scattering indicated as $(g-1)R$ in Eq. (8) has been calculated using (i) the same spectrum $W(E,E_0,t)$ for the electron reaching the target, (ii) the Rosenbluth formula for the elastic e-p cross section, and (iii) the emission of hard photons in the process $e+p\rightarrow e'+p+\gamma$ (wide-angle bremsstrahlung) calculated by Hand.[19] This effect has been found negligible, and g has been assumed to equal 1.

(d) To calculate $E_e(H)$, one needs the contribution from the "external radiator." Because it is small (8% of the real radiator), the contribution is assumed proportional to the thickness of the radiator.

(e) There is still a contribution from an effect called the "ghost proton,"[24] which are the protons which exceed those kinematically allowed by the reaction. Because of the geometry of the experiment, of the kinematical conditions, of the relatively thin target, and of the fact that k/E_0 is close to 1, the contribution is small. It has been estimated to be of the order of 0.05%.

(f) Finally, there is a correction necessary to calculate

[18] T. Janssens, R. Hofstadter, E. B. Hughes, and M. R. Yearian, Phys. Rev. **142**, 922 (1966). If the fit by de Vries *et al.* [Phys. Rev. **134**, B848 (1964)] had been used, results would be changed by 1.1%; i.e., within the accuracy of the measurements.

[19] N. Meister and D. R. Yennie, Phys. Rev. **130**, 1210 (1963); L. N. Hand, Phys. Rev. **129**, 1834 (1963).

[20] E. Segré, *Experimental Nucl. Phys.* (John Wiley and Sons, Inc., New York, 1953), Vol. 1, p. 272.

[21] J. W. DeWire, M. Feldmann, V. L. Highland, and R. Littauer, Phys. Rev. **124**, 909 (1961).

[22] A. P. Contogouris, Phys. Rev. **124**, 912 (1961).

[23] W. Heitler, *Quantum Theory of Radiation* (Clarendon Press, Oxford, 1954), p. 378.

[24] G. Belletini, C. Bemporad, P. L. Braccini, L. Foa, and E. H. Bellamy, Nuovo Cimento **29**, 1195 (1963).

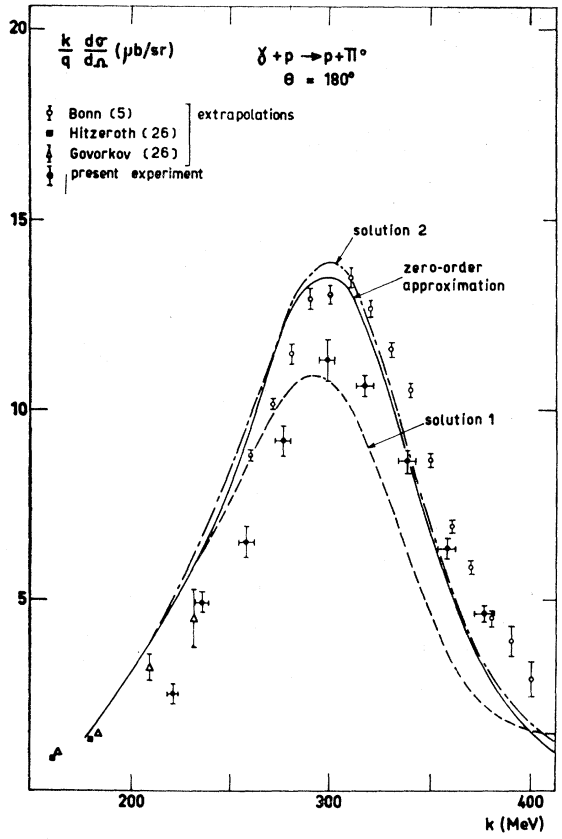

FIG. 5. Comparison between theoretical calculations and experimental results. The results of the Bonn group[5] and of Hitzeroth and Govorkov (see Ref. 26) are extrapolations of measurements made at angles different from $\theta=180°$. Bonn cross sections are taken from a fit of values at different angles according to the expansion of Eq. (1), which is limited to the coefficients A, B, and C. Solid line: zero-order approximation; dashed line: solution 1; dash-dot line: solution 2.

the actual slice Δk of photon energy in the bremsstrahlung spectrum which was effective in producing protons which were transmitted to the detector. This slice depends normally on the Δp setting of the spectrometer through Eq. (11). Because there is a different energy loss for protons of different energy produced at the same point in the target, their Δp after leaving the target is not the same as at the point of production. Therefore, the Δp setting of the spectrometer does not correspond precisely to the Δp needed for the calculation of Δk. This correction was calculated using the energy-loss formula of Sternheimer[25] and tables of Williamson and Boujot.[25] It varied from less than 1% at the highest-energy point to 6% at the lowest-energy point.

VI. EXPERIMENTAL RESULTS AND ERRORS

The summary of the experimental results and errors for the photoproduction of π^0 at 180° (c.m.) is displayed in Table I. The results are presented graphically in Fig. 5 and will be discussed and compared with theoretical predictions in subsequent sections of this paper.

Extrapolated results from the University of Bonn[5] are also shown in Fig. 5 and will be discussed in section VIID. Calculations to fit the data have been made on the Bonn angular distributions. They have been fitted by an expansion including A, B, C, and D coefficients. The extrapolated results for 180° do not differ significantly from the ones which use only A, B, and C. Therefore the discrepancy between the Bonn results and ours cannot be attributed to a big value of the D coefficient. New measurements are scheduled for angles between 90° and 180° to find out the origin of the discrepancy. In Table I, the first column gives the incident beam energy through the relation $k/E_0=0.85$. The second column is the width Δk of the photon beam energy. Column 3 is the π^0 photoproduction cross section measured in the present experiment. Columns 4 and 5 give the statistical errors of the cross sections, absolute and relative, respectively. Columns 6 and 7 refer to the quantities $(k/q)(d\sigma/d\Omega)^*$ and the corresponding absolute errors. They are the values plotted in Fig. 5.

The errors (standard deviations) contain the statistical errors on the counts accumulated during the measurements of the photoproduction cross sections, uncertainties in the elastic e-p scattering for absolute calibration, and the fluctuation of the calibration of the beam monitor during these measurements.

There are also systematic errors which are the same for all points, and which are composed of uncertainties of the bremsstrahlung calculation (2%), energy calibration of the spectrometer (and energy loss of protons in target) (1%),[25] radiator thickness (0.8%), and integrator capacities (0.2%). Finally there is a 3% error of the absolute elastic electron-proton scattering cross section which must be included due to the errors of the proton form factors.

Electroproduction measurements are being analyzed and the results will be published later.

TABLE I. π^0 photoproduction experimental results and errors. The pion angle θ is 180° in the c.m. system.

k (MeV)	Δk (MeV)	$d\sigma^*/d\Omega^*$ (μb/sr)	Absolute error (μb/sr)	Relative error (%)	(k/q) $d\sigma^*/d\Omega^*$ (μb/sr)	Absolute error
221.4	±2.8	2.06	±0.17	±8.2	2.8	±0.23
236.9	±3.0	3.83	±0.22	±5.7	4.96	±0.28
258.4	±3.2	5.30	±0.14	±2.6	6.56	±0.17
276.2	±3.4	7.62	±0.29	±3.8	9.16	±0.35
298.2	±3.8	9.67	±0.45	±4.6	11.29	±0.52
317.6	±4.0	9.30	±0.21	±2.3	10.67	±0.24
339.0	±4.5	7.69	±0.32	±4.1	8.67	±0.36
359.8	±4.8	5.61	±0.29	±5.1	6.25	±0.32
377.3	±5.1	4.2	±0.30	±7.1	4.62	±0.33

[25] C. Williamson and J. P. Boujot, Centre d'Etudes Nucléaires de Saclay Report No. CEA 2189, 1962, (unpublished). R. M. Sternheimer, Phys. Rev. **103**, 511 (1956).

VII. THEORETICAL PREDICTION AND ANALYSIS OF RESULTS

In this section, the experimental data are compared with the theoretical predictions in such a way that one can see clearly those details of the theoretical approximations which are experimentally checked by the $\theta=180°$ excitation curve. The present experimental results will be analyzed along the following lines:

(1) First, we shall calculate an absolute "zero-order prediction" for the $\theta=180°$ excitation curve and establish the discrepancy $\Delta_{\rm exp}(E)$ defined by

$$\Delta_{\rm exp}(E)=(k/q)\{[d\sigma(E,\theta)/d\Omega]_{\rm exp}-[d\sigma(E,\theta)/d\Omega]_{\rm theor}\}. \quad (14)$$

(2) For a reasonable choice of the zero-order amplitude, the discrepancy $\Delta_{\rm exp}$ should arise primarily from small deviations in the $J=\frac{1}{2},\frac{3}{2}$ partial amplitudes which give the largest contribution to $d\sigma/d\Omega$. In the second step we shall therefore study the variation of $d\sigma/d\Omega$ when the first partial amplitudes are altered somewhat, and try to find the origin of the discrepancies.

(3) The information from one excitation curve is of course not sufficient for a complete and unambiguous determination of all necessary corrections. But it turns out that one main reason for the disagreement is connected with the partial amplitudes of the P_{33} resonance. In the final step, the theoretical prediction for the multipoles of the P_{33} resonance will be improved to modify the original zero-order approximation to yield better agreement.

A. Zero-Order Approximation

In Fig. 5 the theoretical prediction is compared with the results of this and other experiments.[5,26] The zero-order amplitude is calculated according to the isobar approximation in the framework of dispersion theory[27,28] modified in two ways:

(1) All $J=\frac{1}{2},\frac{3}{2}$ multipoles except $E_{1+}^{3/2}$ fulfill unitarity (for the standard notation $M_{l\pm}^{I}$ of the multipoles, see Refs. 29 and 27).

(2) The dispersion contribution of $\mathrm{Im}E_{0+}^{1/2}$ and $\mathrm{Im}E_{0+}^{3/2}$ is included. In detail this means:

(a) The resonant multipole $M_{1+}^{3/2}$ is approximated using the result of Chew *et al.*[29]

$$M_{1+}^{3/2}\approx(M_{1+}^{3/2})_{\mu}=\frac{\mu_V}{f}\frac{k}{q}\frac{e^{i\delta_{1+}^{3/2}}\sin\delta_{1+}^{3/2}}{q}, \quad (15)$$

where k and q are the linear momenta of the photon and the pion in the c.m. system, $\mu_V=\frac{1}{2}(g'_P+1-g_N)e/2M$ is the total isovector magnetic moment, $f^2=0.080$ is the pion-nucleon coupling constant, and $\delta_{l\pm}^{I}$ is the pion-nucleon scattering phase shift.

(b) All other real parts of the amplitudes are approximated by retaining only $\mathrm{Im}M_{1+}^{3/2}$, $\mathrm{Im}E_{0+}^{1/2}$, and $\mathrm{Im}E_{0+}^{3/2}$ in the fixed-momentum-transfer dispersion relations.[27,30] $\mathrm{Im}M_{1+}^{3/2}$ is taken from the relationship (14) and $\mathrm{Im}E_{0+}^{1/2,3/2}$ from the Watson theorem,

$$\mathrm{Im}M_{l\pm}^{I}=\mathrm{Re}M_{l\pm}^{I}tg\delta_{l+}^{I}. \quad (16)$$

To apply Eq. (16) for $\mathrm{Im}E_{0+}^{1/2,3/2}$, we used the experimental values for the pion-nucleon phase shift and took $\mathrm{Re}E_{0+}^{1/2,3/2}$ from the following formula:

$$\mathrm{Re}E_{0+}^{1/2,3/2}(W)=E_{0+}^{1/2,3/2}(W)_{\rm p.t.c.}+g_M\times K^{1/2,3/2}(W,\langle W\rangle=8.87), \quad (17)$$

with g_M given by

$$g_M=-\frac{1}{\pi}\int_{M+1}^{\infty}dW\frac{\mathrm{Im}M_{1+}^{3/2}(W)}{qk}. \quad (18)$$

Equation (17) follows from the projected fixed-t dispersion relations if only $\mathrm{Im}M_{1+}^{3/2}$ is retained in the sharp-resonance approximation.[31] $K(W,W')$, taken from Ref. 32, is a known function describing the coupling of $\mathrm{Im}M_{1+}^{3/2}$ to E_{0+} via the dispersion relations, and the index "p.t.c." denotes the pole-term contribution which can also be found in Ref. 32. The result for $\mathrm{Im}E_{0+}^{1/2,3/2}$ following from Eqs. (16) and (17) agrees within a few percent with the iterated result of Donnachie and Shaw.[33] Compared to the case where only $\mathrm{Im}M_{1+}^{3/2}$ is retained in the fixed-t dispersion integrals the inclusion of $\mathrm{Im}E_{0+}^{1/2,3/2}$ has the particular effect of reducing $\mathrm{Re}E_{0+}^{\pi^0}$ by a factor two in the threshold region. The new values for $\mathrm{Re}E_{0+}^{\pi^0}$ are in good agreement with the multipole analysis[34] of the recent data in Ref. 27 in the threshold region.

(c) The imaginary parts of all $J=\frac{1}{2},\frac{3}{2}$ multipoles except $E_{1+}^{3/2}$ are calculated from the Watson theorem (16) and the $\mathrm{Re}M_{l\pm}$ are taken in the approximation (b).

In the above approximation (b), $\mathrm{Re}E_{1+}^{3/2}$ is practically given by the contribution of the pole term, and is therefore not zero at the resonance ($\delta_{1+}^{3/2}=\pi/2$). Therefore, relationship (16) cannot be applied to $E_{1+}^{3/2}$ in the region of the resonance so that we put $\mathrm{Im}E_{1+}^{3/2}=0$ in the zero-order approximation.

In Table II the values for the $J=\frac{1}{2},\frac{3}{2}$ multipoles are given at $E=400$ MeV to demonstrate the order of magnitude of the different contributions. We note further that in the backward direction, only the helicity amplitude $f_{1/2,-1/2}(E,\theta)$ contributes, in which the multipole

[26] W. Hitzeroth, in Proceedings of the International Conference on Low and Intermediate Energy Electromagnetic Interactions at Dubna, 1967 (unpublished); and (private communication).
[27] W. Schmidt, Z. Physik, **182**, 76 (1964).
[28] G. Höhler, Springer Tracts in Modern Phys. **39**, 55 (1965).
[29] G. F. Chew, M. L. Goldberger, F. E. Low, and Y. Nambu, Phys. Rev. **106**, 1345 (1957).
[30] J. S. Ball, Phys. Rev. **124**, 2014 (1961).
[31] J. Engels, W. Schmidt, and G. Schwiderksi, Gesellschaft für Kernforschung, Karlsruhe, 1967, External Report 3/67-1 (unpublished).
[32] W. Schmidt and G. Schwiderski, Fortschr. Physik (to be published).
[33] A. Donnachie and G. Shaw, Ann. Phys. (N. Y.) **37**, 333 (1966).
[34] A. Müllensiefen, Karlsruhe Report, 1967 (unpublished).

TABLE II. Multipoles (in units $10^{-2}\lambda$) at $E=400$ MeV in the zero-order approximation.

	Re $M_{1\pm}$	Im $M_{1\pm}$
E_{0+}	−0.40	0.38
M_{1-}	−0.54	0.06
E_{1+}	0.01	−0.01
M_{1+}	−1.06	1.33
E_{2-}	−0.14	0.00
M_2	0.00	0.00

E_{1+} is kinematically enhanced by a factor 3 among the $l=0$ and 1 multipoles $M_{l\pm}$ which give the largest contribution:

$$\tfrac{1}{2}\sqrt{2}f_{1/2,\,-1/2}(E,\pi)=E_{0+}+M_{1-}-M_{1+}$$
$$-3E_{1+}+E_{2-}-3M_{2-}+6E_{2+}+3M_{2+}+\cdots, \quad (19)$$

with

$$(k/q)[d\sigma(E,\pi)/d\Omega]=\tfrac{1}{2}|f_{1/2,-1/2}(E,\pi)|^2. \quad (20)$$

B. Analysis of the Discrepancy

We turn now to the analysis of the discrepancy $\Delta_{\rm exp}(E)$ which shows a marked energy dependence and which is already rather large at low energies (Fig. 5). To analyze this discrepancy in detail, we consider the differences (Fig. 6)

$$\Delta\sigma(E,\theta,\Delta M_{l\pm})=(k/q)\{[d\sigma(E,\theta)/d\Omega]_{\rm theor}{}^{*}$$
$$-[d\sigma(E,\theta)/d\Omega]_{\rm theor}\} \quad (21)$$

for the three angles $\theta=0°$, 90°, 180°. In $[d\sigma(E,\theta)/d\Omega]_{\rm theor}{}^{*}$, the isospin $I=\frac{3}{2}$ component of the real or imaginary part *of one* multipole is changed by the amount

$$\Delta\ {\rm Re(Im)}M_{l\pm}{}^{3/2}=0.1\times10^{-2}\lambda,$$

where λ is the Compton wavelength of the pion. The contributions quadratic in $\Delta M_{l\pm}$ are usually negligible in Fig. 6, so that $\Delta\sigma$ is practically proportional to $\Delta M_{l\pm}$. Then the results can also be applied for changes in the $I=\frac{1}{2}$, 0 (isoscalar) or total π^0 amplitude using the approximate relationship

$$\Delta\sigma(\Delta M_{l\pm}{}^{3/2})=0.5\Delta\sigma(\Delta M_{l\pm}{}^{1/2})=1.5\Delta\sigma(\Delta M_{l\pm}{}^{0})$$
$$=1.5\Delta\sigma(\Delta M_{l\pm}{}^{\pi^0}). \quad (22)$$

The changes $\Delta M_{l\pm}$ in Fig. 6 are typical for the uncertainty of the $l=0$ and 1 multipoles E_{0+}, M_{1-}, E_{1+}, M_{1+}.

For $l\gtrsim2$ one can expect considerably smaller corrections of the multipoles, which would not yield the right order of magnitude for the modification of $d\sigma/d\Omega$. Therefore, effects of the right magnitude are to be expected only from alterations in the $l=0$ or 1 multipoles, among which E_{1+} leads to the largest changes in the backward (and forward) direction. It is therefore reasonable to assume that a large part of the discrepancy arises through the multipole E_{1+}, of which we suppose that the $E_{1+}{}^{3/2}$ part (connected with the P_{33} resonance) is the most doubtful input. But one has to realize that, according to Fig. 6, changes in E_{1+} spoil the good agreement for the $\theta=90°$ excitation curve,[27] so that also other multipoles have to be altered to restore the agreement there. But at $\theta=90°$ only modifications in M_{1+} can markedly contribute apart from those in E_{1+}, so that, taken together, the results for $\theta=90°$ and 180° suggest corrections of the multipoles E_{1+} and M_{1+}. It is noteworthy in this context that changes in M_{1+} and E_{1+} of

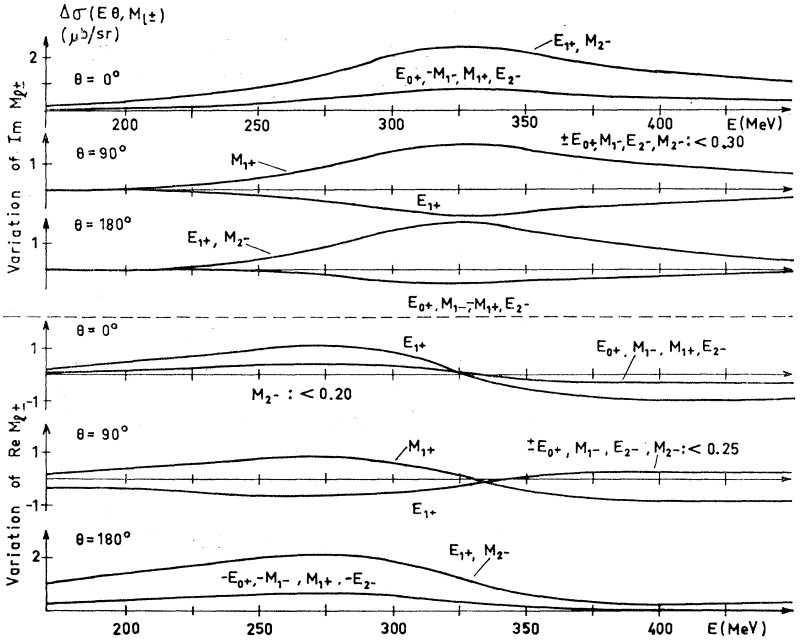

FIG. 6. The variations, $\Delta\sigma(E,\theta,\Delta M_{l\pm})$ (Eq. 14) for $\Delta\ {\rm Re(Im)}M_{l\pm}=0.1\times10^{-2}\lambda$.

the same sign yield contributions of the same sign for $\theta=180°$ and of opposite sign for $\theta=90°$. One can therefore reasonably expect that the discrepancy is mainly affected by the E_{1+} and M_{1+} multipoles, of which the parts connected with the P_{33} resonance have to be examined primarily.

C. Refined Calculations

We consider a dispersion relation for the partial amplitudes of the first resonance,

$$\mathrm{Re}\, H_\lambda(W)=H_\lambda^{i}(W)+(1/\pi)P\int_{M+1}^{\infty}dW'\frac{\mathrm{Im}H_\lambda(W')}{W'-W}, \quad (23)$$

where we have introduced the helicity amplitudes

$$H_{1/2}(W)=(\tfrac{1}{2}\sqrt{2})[3E_{1+}^{3/2}(W)+M_{1+}^{3/2}(W)]/[qkC(W)], \quad (24a)$$

$$H_{3/2}(W)=(\sqrt{\tfrac{3}{2}})[E_{1+}^{3/2}(W)-M_{1+}^{3/2}(W)]/[qC(W)], \quad (24b)$$

with

$$C(W)=(s-M^2/16\pi s)(W+M)^2-1]^{1/2}. \quad (25)$$

$H_\lambda^{i}(W)$ in Eq. (22) represents the inhomogeneous term analytic on the physical cut. An improved solution of Eq. (23) has been attempted recently by various authors[35] trying to find an approximate, but physically meaningful, calculation of the N/D type. The approach of Finkler[35] has been generalized in Ref. 36 to get an exact representation for $H_\lambda(W)$,

$$H_\lambda(W)=|H_\lambda(W)|e^{i\varphi_\lambda}=[N_\lambda(W)/D_\lambda(W)], \quad (26)$$

with

$$D_\lambda(W)=\exp\left[-\frac{1}{\pi}\int_{M+1}^{W_\lambda}dW'\frac{\varphi_\lambda(W')}{W'-W-i\epsilon}\right], \quad (27)$$

$$N_\lambda(W)=H_\lambda^{i}(W)+\mathrm{Re}\, D_\lambda(W)\times[H_\lambda^{i}(W)-H_\lambda^{i}(W_\lambda)]+\Delta N_\lambda(W), \quad (28)$$

and

$$\Delta N_\lambda(W)=-\frac{1}{\pi}\int_{M+1}^{W_\lambda}dW'\frac{\mathrm{Im}D_\lambda(W')}{W'-W}\times[H_\lambda^{i}(W')-H_\lambda^{i}(W_\lambda)]+\frac{1}{\pi}\int_{W_\lambda}^{\infty}dW'\frac{\mathrm{Im}H_\lambda(W')}{W'-W}D_\lambda(W'). \quad (29)$$

Because of the Watson theorem at low energies, the phase $\varphi_\lambda(W)$ is given by $\delta_{1+}^{3/2}$, the pion-nucleon scattering phase shift. W_λ is a cutoff parameter, which has to be chosen so that the high-energy contribution represented by the second integral in Eq. (29) can be neglected for values of W in the region of the first resonance. In practice the energy W_λ lies above the second pion-nucleon resonance $N(1518)$. In the sharp-resonance approximation where

$$\varphi_\lambda(W)=0, \quad W<W_R \qquad =\pi, \quad W>W_R \quad (30a)$$

and

$$D_\lambda(W)=\frac{W-W_R}{W-W_\lambda} \quad (30b)$$

($W_R=8.87m_\pi c^2$, the resonance energy), the first integral of $\Delta N_\lambda(W)$ in Eq. (29) vanishes. This indicates the smallness of this contribution. The main difficulty in an actual calculation of $E_{1+}^{1/2}$ and $M_{1+}^{3/2}$ from Eqs. (27), (28), and (29) becomes clear if we choose the special point $W=W_R$, where one has

$$N_\lambda(W_R)=H_\lambda^{i}(W_\lambda)+\Delta N_\lambda(W_R), \quad (31)$$

since at the resonance

$$\mathrm{Re}D_\lambda(W_R)=|D_\lambda(W_R)|\cos\tfrac{1}{2}\pi=0. \quad (32)$$

The relationship (31) demonstrates clearly that a precise knowledge of the behavior of the inhomogeneous term $H_\lambda^{i}(W)$ above the second resonance is decisive for a reliable prediction of the multipoles $E_{1+}^{3/2}$, $M_{1+}^{3/2}$ around the resonance. In Ref. 36 the inhomogeneous term $H_\lambda^{i}(W)$ has been investigated using the partial-wave expansion of $H_\lambda^{i}(W)$ derived from fixed-momentum-transfer dispersion relations.[32] It has been shown that with increasing energy the contributions of the first and second resonance are important in $H_\lambda^{i}(W)$. But the effect of the second resonance cannot be safely predicted now and the use of a truncated partial-wave expansion for the inhomogeneous term becomes doubtful already at the second resonance.

D. Results

Since no method is known presently that gives a prediction of $H_\lambda^{i}(W_\lambda)$ in Eq. (31) within the errors of $\Delta N_\lambda(W_R)$, both numbers $H_\lambda^{i}(W_\lambda)$ will be considered as free parameters to be fitted to the experimental results. Taking then for $H_\lambda^{i}(W)$ in the region of the first resonance the expression derived from fixed-momentum-transfer dispersion relations, a prediction for $E_{1+}^{3/2}$ and $M_{1+}^{3/2}$ is possible.[36] We choose $W_{1/2}=W_{3/2}=13.022$ $m_\pi c^2$. In Fig. 5 we also show, apart from the zero-order approximation, two results covering the present range of experimental uncertainty and calculated with two solutions [(1) and (2)] for the resonant multipoles. Both results were fitted to the $\theta=180°$ and 90° excitation curves at $E=300$ MeV. At $\theta=180°$ we took our result [solution (1)] and that of Ref. 5 [solution (2)]; at $\theta=90°$ we have chosen as reference again the new results at Bonn,[5] which are in complete agreement with some

[35] P. Finkler, University of California Radiation Laboratory Report No. UCRL-7953-T 1964 (unpublished); W. Korth, H. Rollnik, D. Schwela, and R. Weizel, Bonn Report No. 2-7, 1965 (unpublished); G. Mennessier, Nuovo Cimento 46, 459 (1966); N. Zagury, Phys. Rev. 145, 1112 (1966).

[36] J. Engels and W. Schmidt (to be published).

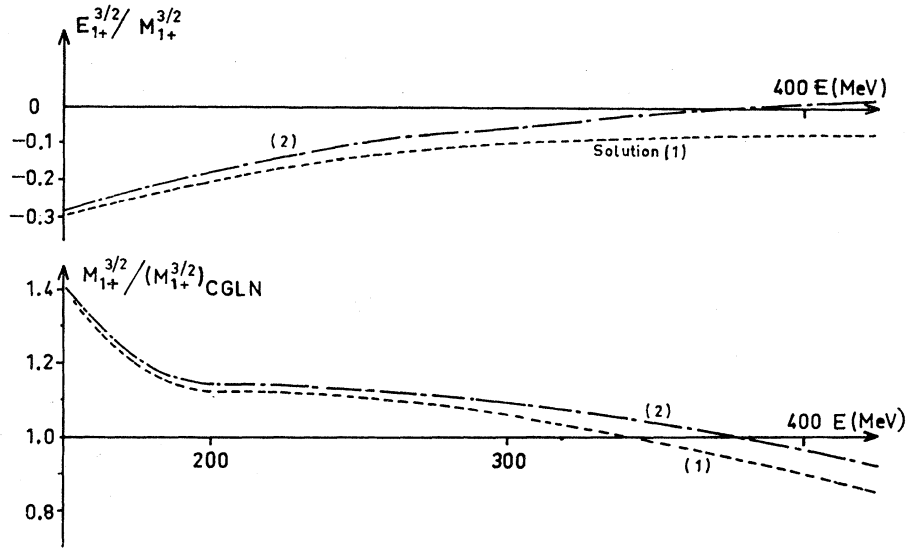

FIG. 7. The ratios $E_{1+}^{3/2}/M_{1+}^{3/2}$ and $M_{1+}^{3/2}/(M_{1+}^{3/2})_{CGLN}$ according to solutions 1 (dashed line) and 2 (dash-dot line).

new preliminary data we took recently and are larger around the resonance by about 10% than the prediction of the zero-order approximation and the older experimental data. From Fig. 5 we conclude that a failure in the prediction of the resonant multipoles cannot be responsible for all discrepancies in the $\theta=180°$ excitation curve. But since the theory of the first resonance gives no absolute prediction, it is not possible to detect the origin of the discrepancies in the other multipoles by the analysis of this particular excitation curve at $\theta=180°$. One should note that the discrepancy is of the order expected from the uncertainty of the $J=\frac{1}{2}, \frac{3}{2}$ multipoles.

The values for the constants $H_\lambda{}^i(W_\lambda)$ for solutions (1) and (2), together with the physically more meaningful values for $\mathrm{Im}M_{1+}{}^{3/2}(W_R)$ and the ratio $E_{1+}{}^{3/2}(W_R)/M_{1+}{}^{3/2}(W_R)$, are displayed in Table III. Also shown (in brackets) are the values for $H_\lambda{}^i(W_\lambda)$ expected from its partial-wave expansion. The deviation from the experimentally found values is noteworthy. In Fig. 7 are presented the ratios

$$E_{1+}{}^{3/2}/M_{1+}{}^{3/2} \quad \text{and} \quad M_{1+}{}^{3/2}/(M_{1+}{}^{3/2})_{\mathrm{CGLN}}$$

TABLE III. The inhomogeneous terms, fitted and expected (in parentheses) at $W_{1/2}=W_{3/2}=13.022\ m_\pi c^2$ and the corresponding multipoles (units $10^{-2}\ \lambda$) near the resonance at $E=340$ MeV.

Solution	$H_{1/2}{}^i$	$H_{3/2}{}^i$	Im $M_{1+}{}^{3/2}$	$E_{1+}{}^{3/2}/M_{1+}{}^{3/2}$
(1)	0.30 (0.37)	−1.57 (−1.93)	3.40	−0.09
(2)	0.40 (0.39)	−1.56 (−1.91)	3.55	−0.03

for the two different solutions, where $(M_{1+}{}^{3/2})_{\mathrm{CGLN}}$ is the result for $M_{1+}{}^{3/2}$ according to Eq. (15). It should be noted that all solutions for $E_{1+}{}^{3/2}$ differ mainly with increasing energy and that the maximum of $M_{1+}{}^{3/2}$ is shifted to lower energies.

The present analysis has established the importance for an improved absolute prediction for the multipoles $E_{1+}{}^{3/2}$, $M_{1+}{}^{3/2}$ of the first resonance and for $\mathrm{Re}E_{0+}{}^{\pi^0}$, the prediction of which suffers in both cases from unknown high-energy contributions to the corresponding solutions. The result for $\mathrm{Re}E_{0+}{}^{\pi^0}$ relies strongly on the choice of the cutoff parameter around $E=800$ MeV in the fixed-t dispersion relations. Therefore it will be one of the tasks for future theoretical developments to circumvent these difficulties.

ACKNOWLEDGMENTS

We wish to thank Professor A. Blanc-Lapierre and the staff of the Accélérateur Linéaire, Orsay, for the help we have received during all the stages of this experiment. We also thank Dr. E. Erickson for taking an active part in the last phase of the work and for many useful discussions. One of us (E. D.) wishes to acknowledge the welcome and the generous support of Professor S. Gorodetzky in his laboratory at Strasbourg. We are indebted to Professor B. Govorkov, Dr. W. Hitzeroth, and Professor G. Knop for communicating their results before publication. We thank Dr. A. Mullensiefen for several discussions and J. Engels for his aid in the theoretical computations.